

CONVECTIVE EFFECTS DURING DIFFUSIVITY MEASUREMENTS IN LIQUIDS WITH AN APPLIED MAGNETIC FIELD

Yu Yu Khine¹, R. Michael Banish^{1,2}, and J. Iwan D. Alexander³

¹University of Alabama in Huntsville, Huntsville, Alabama 35899, U.S.A.

²To whom correspondence should be addressed.

³Case Western Reserve University, Cleveland, Ohio 44106, U.S.A.

Abstract

Convective contamination of self-diffusion experiments with an applied magnetic field is considered using a two-dimensional axisymmetric model. Constant, uniform, and an additional non-uniform heat fluxes are imposed along the sidewall of the cylinder while constant heat loss occurs through the top and bottom. In this model, due to a very small thermal Peclet number, convective heat transfer is neglected, and the flow is steady and inertialess. Time-dependent concentration is solved for various values of the mass Peclet number, Pe_m , (the ratio between the convective transport rate and the diffusive transport rate) and different magnetic field strengths represented by the Hartmann number Ha . Normalized values of these diffusivities vs. effective Pe_m are presented for different imposed temperature profiles. In all cases, the diffusivity value obtained through the simulated measurement increases as the effective Pe_m increases. The numerical results suggest that an additional periodic flux, or “hot” and “cold” spots, can significantly decrease the convective contamination in our geometry.

1. Introduction

During liquid self-diffusion experiments, a small non-uniformity in temperature within the melt may drive buoyant convection. This convection can result in erroneous values of the measured diffusivity. Verhoeven [1] emphasized that any horizontal component of a density gradient in the liquid results in spontaneous convection with no threshold. Alexander et al. [2] showed that for three-dimensional (3D) time-dependent transport in the presence of gravity with horizontal temperature non-uniformities across the sample as low as 1 and 0.1 K, convective transport rates in 1 and 3 mm capillaries, respectively, can exceed diffusive transport rates, and, thus, result in higher values of measured diffusivities. Alexander and Banish [3] presented the results of combined numerical modeling and order-of-magnitude estimates of the sensitivity of convective contamination to low-gravity in self-diffusion experiments.

Applied magnetic fields have been used to suppress the buoyant convection in the liquid metals and semiconductors due to their large electrical conductivities [4-6]. Youdelis et al. [7] showed that at high magnetic field strengths, the diffusion process itself can be significantly modified through the Lorentz body force acting on the conducting liquids ions and electrons. Alboussiere et al. [8] found that with electromagnetic damping the convective contribution to the effective mass Peclet number is scaled as Hartmann number Ha^{-4} .

Keywords: self-diffusivity, convection, magnetic fields, thermal asymmetries, flight

*Corresponding author. email: banishm@email.uah.edu

In actual self-diffusivity experiments, measured diffusivity results that deviate by less than 5% from the (known) real value, D_o , would be considered “acceptable. The purpose of this paper is to quantitatively estimate the magnitude of allowable temperature non-uniformities in the liquid that will guarantee that measured diffusivity values lie within 5% of the actual value when the experimental system is subject to an axial magnetic field. To model the experiment, axisymmetric, time-dependent transport due to a combination of steady flow and diffusion is considered. In this basic model, a steady, uniform heat flux that produces a radial temperature difference in the liquid is imposed on the sidewall of the cylindrical container while uniform heat losses are imposed on the top and bottom walls. Then, a steady, spatially-periodic heat flux is superimposed on the sidewall of the cylinder to predict the effect of spatial temperature variations which represent the localized hot and cold spots along the sidewall. Note that the overall flux for this additional periodic condition is zero. Simulated diffusivity results for two different magnetic field strengths and five various temperature profiles along the sidewall are presented in this paper.

2. Problem Formulation

In this model, a Boussinesq fluid contained in a closed vertical circular cylinder of length $Z = 30$ mm with an inside radius R of 1.5 mm. Gravity acts downward along the cylinder axis while a uniform axial magnetic field is applied in the opposite direction as in Fig. 1a. The origin lies at ($R = 0$) and $z = Z/(2R)$. The isopicnic radioactive tracer is initially located at the bottom of the cylinder. The dimensionless model has the top and bottom limits of $z = 10$ and -10 , respectively, while the vertical wall lies at $r = 1$.

2.1. Thermal Problem

For sufficiently large values of magnetic field strength B , the magnetic damping results in a characteristic ratio of convective to conductive heat transfer (the thermal Péclet number, $Pe = \rho c_h UR/\lambda$, where ρ is uniform density, c_h is the specific heat, U is a characteristic velocity and λ is the thermal conductivity) is small; the dimensionless temperature in this case is then governed by $\nabla^2 T = 0$. Therefore, in this model, we assume that convective heat transfer is negligible (i.e., $Pe \ll 1$) and that a uniform heat flux density is imposed along the vertical wall and constant heat losses through the top and bottom walls of the cylinder with the possibility of an additional spatially-periodic heat flux of various amplitude and wavelength on the vertical sidewall in some cases. With these assumptions, the energy equation ($\nabla^2 T = 0$) is non-dimensionalized by R for length and $2\Delta T_r$ for temperature, where ΔT_r is the temperature difference between the centerline and the vertical (side) wall and the dimensionless analytical solution for temperature is

$$T(r, z) = s_1 \left(\frac{r^2}{2} - z^2 \right) + s_2 I_0(ar) \cos(az), \quad (1)$$

where $a = n\pi/10$ and n is a known integer, s_1 and s_2 are set coefficients, and I_0 is a modified Bessel function of the first kind of order zero. The first term on the right hand side of Eq. (1) represents the temperature distribution due to a uniform heat flux while the second term represents the temperature distribution due to a spatially-periodic heat flux.

2.2. Flow Problem

At sufficiently large values of B , the characteristic ratio of the electromagnetic body force to the inertial effect (the interaction parameter, $N = \sigma B^2 R / (\rho U)$, where σ is the electrical conductivity of the liquid) is very large and, thus, the inertial terms in the Navier-Stokes equations become negligible. In addition to the applied magnetic field produced by the magnet, associated electric currents induce an additional magnetic field since the materials considered here are electrically conducting. The characteristic ratio of

the induced to applied magnetic field strengths is the magnetic Reynolds number, $R_m = \mu_p \sigma UR$, (where μ_p is the magnetic permeability of the liquid) and this is very small for crystal growth processes and self-diffusion experiments of liquid metals and semiconductors. Thus, neglect of the induced magnetic field effect is justifiable in the model presented here.

Khine and Walker [9] determined the characteristic velocity for magnetically damped axisymmetric buoyant convection $U = 2\rho g_0 \beta \Delta T_r / (\sigma B^2)$, where g_0 is the gravitational acceleration (9.81 m/s²) and β is the volumetric expansion coefficient for Boussinesq approximation, and this is used to non-dimensionalize the velocity. The magnetic flux, reduced pressure (the difference between the total pressure and the hydrostatic pressure) with uniform density, the electric current density, and the electric potential are non-dimensionalized using B , $\sigma UB^2 R$, σUB , and UBR , respectively. The dimensionless, inertialess equations governing the steady, axisymmetric buoyant convection are then

$$\nabla \cdot \mathbf{v} = 0, \quad (2a)$$

$$\nabla p = T \hat{z} + \mathbf{j} \times \hat{z} + Ha^2 \nabla^2 \mathbf{v}, \quad (2b)$$

$$\nabla \cdot \mathbf{j} = 0, \quad (2c)$$

$$\mathbf{j} = -\nabla \phi + \mathbf{v} \times \hat{z}. \quad (2d)$$

Here, $Ha = BR(\sigma/\mu)^{1/2}$, where μ is the viscosity of the liquid, Eq. (2a) is the conservation of mass, Eq. (2b) is the Navier-Stokes equation with a buoyancy force and an electromagnetic body force, Eq. (2c) is the continuity of electric current density \mathbf{j} , and Eq. (2d) is Ohm's law with an electric potential function ϕ . We eliminated the pressure p , by introducing a stream function, $\psi(r, z)$ which satisfies Eq. (2a).

The boundary conditions are

$$\psi = \frac{\partial \psi}{\partial r} = 0, \text{ at } r = 1; \quad (3a)$$

$$\psi = 0, \text{ at } z = -10, 10. \quad (3b)$$

We used the Chebyshev spectral collocation method to solve the equation governing $\psi(r, z)$.

2.3. Diffusion Problem

The dimensionless axisymmetric governing equation for diffusion is

$$\frac{\partial c}{\partial t} + Pe_m \mathbf{v} \cdot \nabla c = \nabla^2 c. \quad (4a)$$

Here, t is normalized by the diffusion time scale (R^2/D_0) and c is scaled by the initial concentration C_0 . $Pe_m = UR/D_0$ is the characteristic ratio of convective effects to diffusive effects in the process. Here, U is the calculated characteristic velocity and differs from case to case. Since there is no mass transfer across any boundary, the boundary conditions are

$$\frac{\partial c}{\partial r} = 0, \text{ at } r = 1; \quad (4b)$$

$$\frac{\partial c}{\partial z} = 0, \text{ at } z = -10, 10. \quad (4c)$$

Eq. (4a) is solved for different Pe_m with conditions (4b, 4c) using a Chebyshev spectral collocation method for spatial discretization as in the flow problem while conventional finite-difference is used for temporal discretization.

The initial condition for c where tracer forms a thin layer at the bottom of the cylinder is represented by

$$c(r,z,t=0) = \exp(-\alpha(z+10)^2), \quad (5)$$

where $\alpha = 3$ and dramatically to $c \approx 0$ around $z = -9$. The simulated measurements (or output diffusivities D) are computed from the resulting time traces of concentration through a straight line fit in the form,

$$\ln[c_1(t) - c_2(t)] = \text{constant} - \left(\frac{\pi^2 D}{Z^2} \right) t \quad (6)$$

which is known as Codastefano [11] or Harned [12] technique. c_1 and c_2 are concentration measured at $z = Z/6$ and $5Z/6$ along the length of the cylinder, respectively, and the *constant* depends on the concentration profile $c(z)$ at $t = 0$.

In the flow problem, 15 collocation points are needed in the radial direction and 40 points in the axial. In the diffusion problem, the total number of collocation points in r is 15 and that in z is 80 since the entire cylinder is considered. Liquid indium with $\beta = 1.02 \times 10^{-4} \text{ K}^{-1}$, $\rho = 6.64 \times 10^3 \text{ kg} \cdot \text{m}^{-3}$ and $\sigma = 3.02 \times 10^6 \text{ S} \cdot \text{m}^{-1}$ [13] is used as a model fluid. A self-diffusivity value of $D_0 = 1.48 \times 10^{-5} \text{ cm}^2 \cdot \text{s}^{-1}$ was used as the input. Two different Hartmann numbers are considered. For liquid indium these correspond to magnetic field strengths of 0.218 T ($Ha = 25$) and 0.873 T ($Ha = 100$). The characteristic diffusion time is 1520 s, and values of Pe_m between 0 and 4 are considered here.

3. Results and Discussion

The results for five different incoming heat fluxes (see Figs. 1b to 1f) are presented in this section. Case I presents self-diffusion with a radial temperature difference only as the driving force in the liquid due to the steady, uniform heat flux along the sidewall. Cases II through V present self-diffusion with various magnitude of uniform heat flux and superimposed, steady, spatially-periodic heat flux with various amplitude and wavelength along the sidewall (i.e., localized hot and cold spots along the sidewall in addition to the radial temperature difference in the liquid). The desired incoming heat fluxes for Cases I through V are obtained by adjusting s_1 , s_2 and a in Eq. (1). Table I presents summarized results for those five different cases.

Case I: $s_1 = 1$ and $s_2 = 0$ in Eq. (1)

In this case, a uniform heat flux of density 1 that produces a radial temperature difference in the liquid is applied through the vertical wall with uniform heat loss through the top and bottom end walls as in Fig. 1b. The isotherms show symmetry from $z = 0$ plane, and are slightly deviated from the horizontal, and decrease toward the top and bottom walls. The streamlines for both Ha circulate in counterclockwise motion beginning near the vertical wall.

Figure 2 presents the diffusivity vs. effective Pe_m for $Ha = 25$ and 100. For both Ha , the results lie on one curve that bows upward as the effective Pe_m increases. From the results, we can see that the convective effect is extremely large for a larger effective Pe_m . For effective $Pe_m < 2$, the predicted convective effect in self-diffusivity measurements (i.e., difference in diffusivity from D_0) is less than 5% for both $Ha = 25$ and 100. The allowable driving force ΔT_r for $Ha = 25$ is about 0.00373 K while that for $Ha = 100$ is about 0.00501 K to prevent convective contamination in excess of 5%.

Case II: $s_1 = s_2 = 1$ and $n = 3$ in Eq. (1)

In this case, the uniform heat flux is the same as in Case I which produces a radial temperature difference in the liquid while a periodic flux with an amplitude of 0.495 is superimposed at the sidewall to produce the localized periodic temperature variation effect. Here, $n = 3$ represents the number of periodicity in the non-uniform heat flux. The maxima of the periodic flux occur at $z = -6.67, 0$ (mid-plane), and 6.67 while the minima occur at $z = -10$ (bottom wall), $-3.33, 3.33$, and 10 (top wall). So, the top and bottom walls, $z = Z/6$ and $5Z/6$ are slightly cooler than the rest of the cylinder.

For Case II, the diffusivity results are plotted in Fig. 3 for both values of Ha . Again, the two curves bow upward as the effective Pe_m increases. The curve for $Ha = 100$ is slightly higher than that for $Ha = 25$. The difference is more obvious at a larger effective Pe_m . For the diffusivity results of less than 5% deviation from D_0 , the allowable ΔT_r for $Ha = 25$ is 0.00373 K and that for $Ha = 100$ is 0.00548 K. Case II results are very close to those of Case I. The spatially-periodic temperature along the sidewall does not affect the diffusivities significantly although the presence is observed in the flow pattern.

Case III: $s_1 = 0.01, s_2 = 1$, and $n = 3$ in Eq. (1)

As shown in Fig. 1d, the uniform heat flux with a magnitude of 0.01 (i.e., 100 times smaller than that in Case I) and a spatially-periodic flux with an amplitude of 0.495 (same as in Case II) are imposed at the sidewall. For Case III, the consequences of the magnetic field for transport can be seen from the diffusivity vs. the effective Pe_m shown in Fig. 3. For both Ha , the curves bow upward as the effective Pe_m increases. The effect of convection on the measured diffusivity is more prominent at a larger effective Pe_m . Also, the diffusivity curve for $Ha = 100$ lies above the curve for $Ha = 25$. For less than 5% deviation from D_0 , the driving ΔT_r for $Ha = 25$ is about 0.0249 K while for $Ha = 100$, it is 0.171 K. Thus, Case III suggests that reducing the radial temperature gradient in the liquid by 100 times from its original value (as in Case I) has a tremendous effect on the diffusivity results for this model. The effect is more prominent at higher Ha for this case (i.e., at stronger magnetic field strength).

Case IV: $s_1 = 0.001, s_2 = 1$, and $n = 3$ in Eq. (1)

Here, the uniform heat flux which produces a radial temperature difference in the liquid is further reduced to a magnitude of 0.001 (i.e., 10 times less than that in Case III and 1000 times less than that in Case I) while keeping the periodic temperature profile unchanged as in Cases II and III. The diffusivity vs. effective Pe_m for Case IV is shown in Fig. 3 for both Ha . As in the previous case, the two curves bow upward as the effective Pe_m increases, and the curve for $Ha = 100$ is higher than that for $Ha = 25$, especially at larger effective Pe_m . The allowable ΔT_r in this case for $Ha = 25$ is 0.0262 K while that for $Ha = 100$ is 0.184 K which is a slight improvement from those in Case III. Thus, reducing the magnitude of radial temperature gradient by 10 times from Case III does not result in tremendous changes in diffusivity results.

Case V: $s_1 = 0.01, s_2 = 1$, and $n = 2$ in Eq. (1)

This case is the same as Case III except $n = 2$ here so that the isotherms decrease and increase two times alternatively in between the top and bottom walls (i.e., the periodicity is 2 here). The uniform flux which produces the radial temperature difference is 100 times smaller than that in Case I. The maxima of spatially-periodic flux occur at $z = -10$ (bottom wall), 0 (mid-plane), and 10 (top wall) with a magnitude of 0.207 while the minima occur at $z = -5$ and 5 . So, the top and bottom walls and the mid-plane are slightly warmer than the rest of the cylinder.

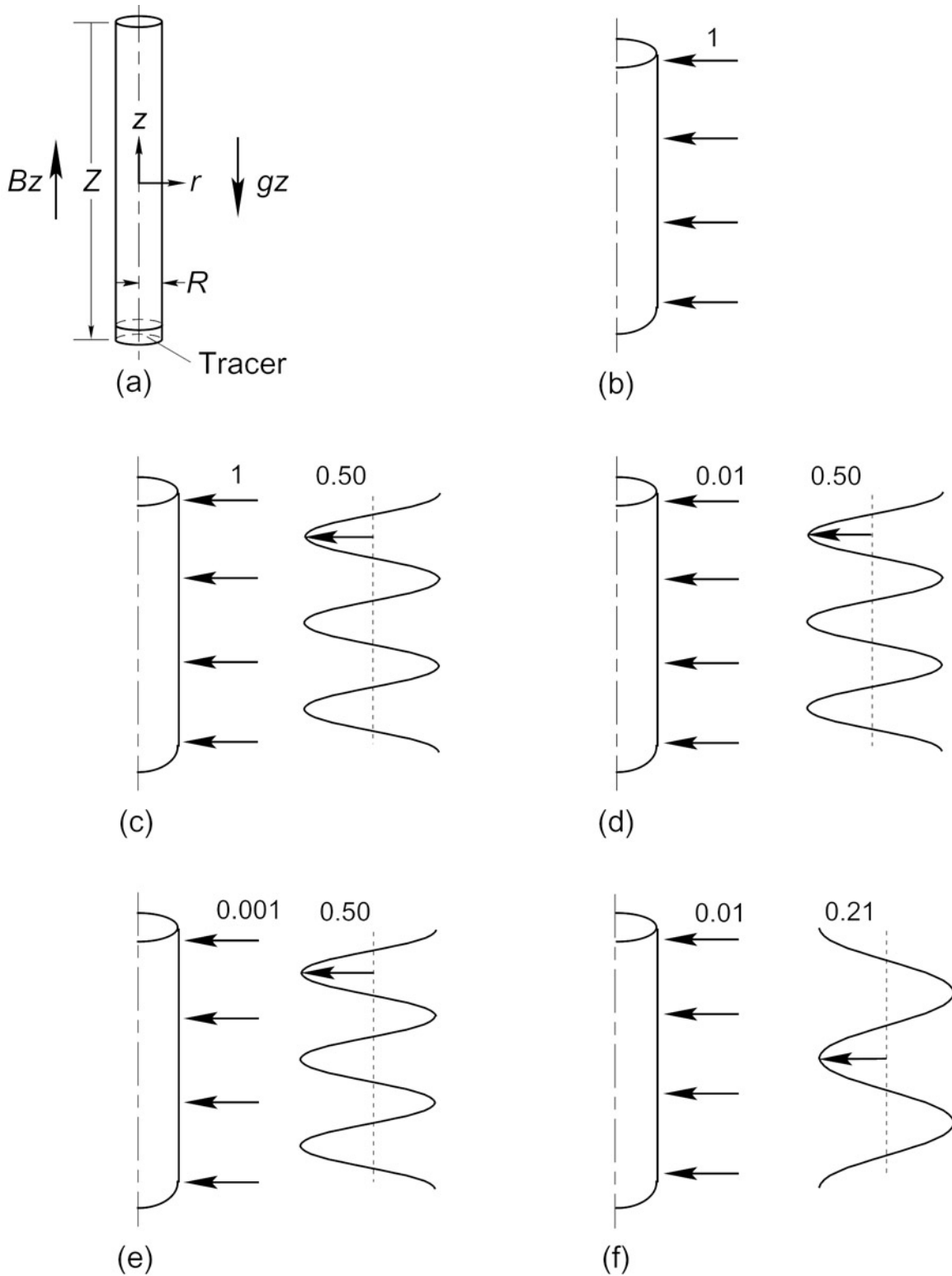


Fig. 1 Model diffusion capillary. Fig. 1a presents the set up and Figs. 1b - 1f describe the dimensionless incoming heat fluxes for Cases I through V.

The diffusivities vs. effective Pe_m for Case V are plotted in Fig. 3 for both Ha . The curve for $Ha = 100$ is higher than that for $Ha = 25$ and the convective effects are more obvious at larger effective Pe_m . In this case, the allowable temperature non-uniformity ΔT_r for $Ha = 25$ is $0.0426 K$ and that for $Ha = 100$ is $0.222 K$. The results are close to those of Case III with an improvement in sensitivity of allowable temperature for the same magnetic field strength.

4. Conclusions

The use of an axial magnetic field to offset the detrimental effects of convection on diffusivity measurements in liquid metals has been examined using a numerical model. Our goal was to determine what magnetic field strengths would be necessary given various temperature non-uniformities to ensure that convective transport was less than 5% of the diffusive. Two different flow patterns were observed for the various imposed temperature non-uniformities. For a uniform heat flux along the sidewall that produces a radial temperature difference in the liquid, the streamlines form a counterclockwise motion. For a spatially-periodic heat flux which produces the localized hot and cold spots on the vertical wall, the flow is arranged as vertically stacked cells and the number of cells depends on the periodicity of the temperature profile due to periodic flux.

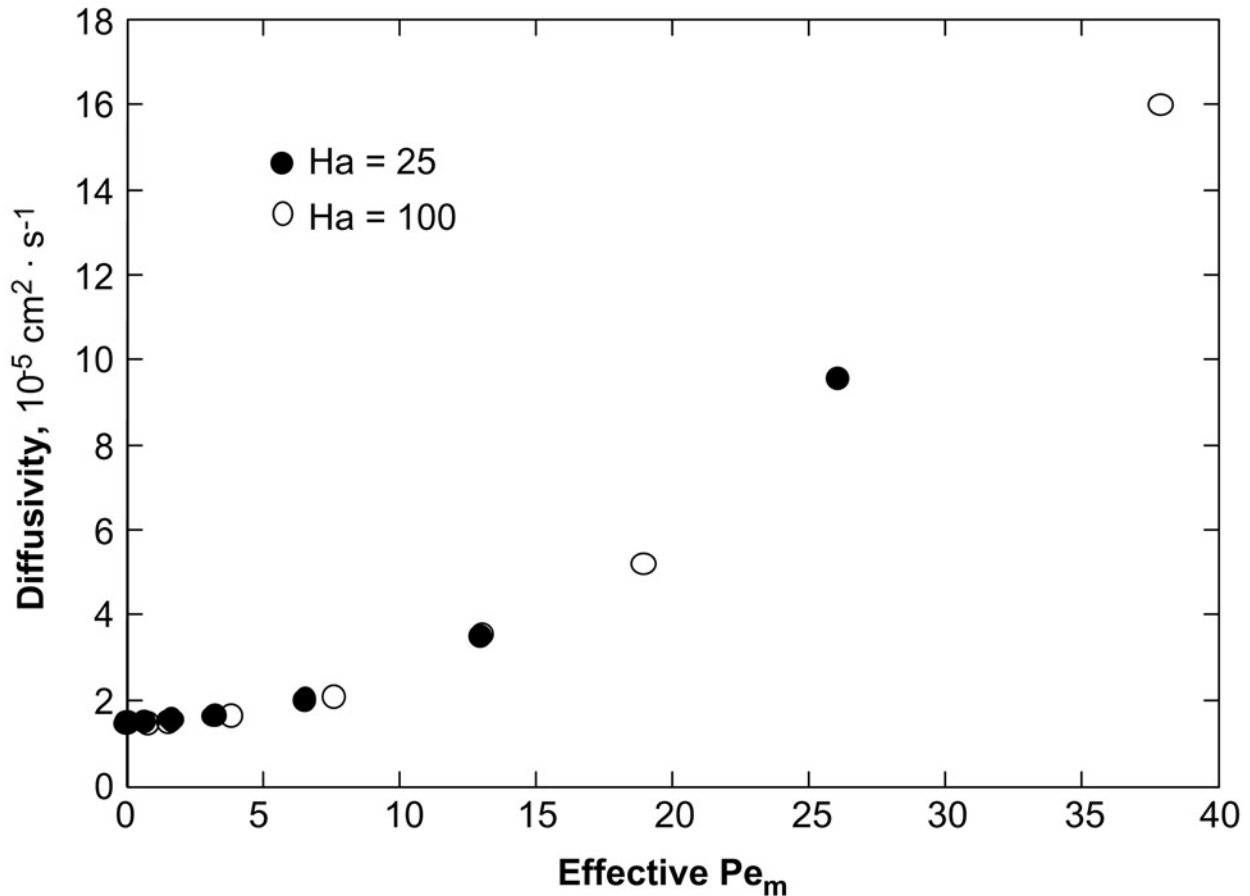


Fig. 2 Diffusivity vs. effective Pe_m for Case I.

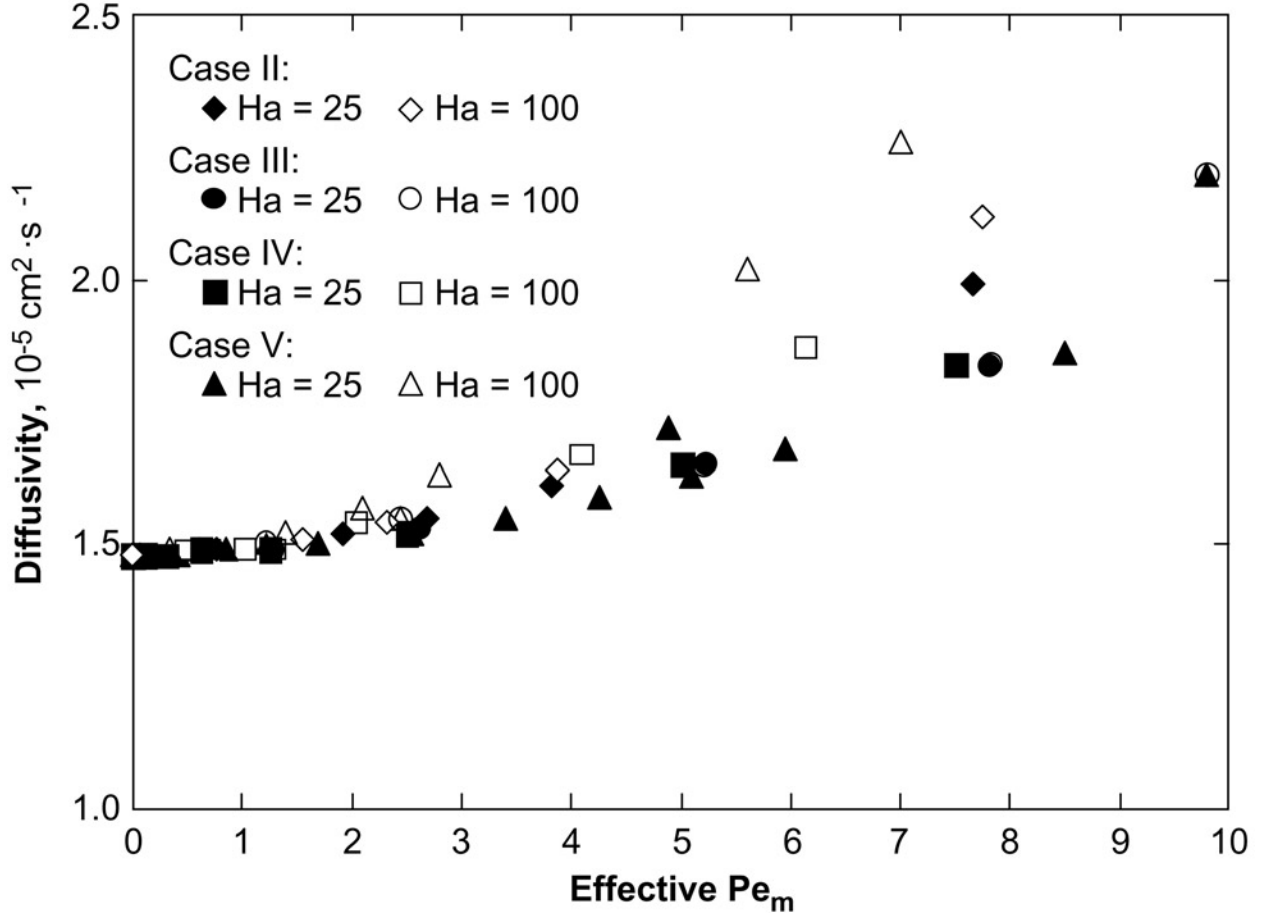


Fig. 3 Diffusivity vs. effective Pe_m for Cases II, III, IV and V.

Table 1. Summary of results for Cases I – V.
Case I: uniform heat flux only; $d=1$, $e=0$ in Eq. (1)

$B = 0.218T$	ΔT_r (K)	$ v_{r \max} $ (cm/s)	$ v_{z \max} $ (cm/s)	U (cm/s)	effective Pe_m	$D \times 10^5$ (cm^2/s)
$Ha = 25$	0.00107	7.34×10^{-6}	6.42×10^{-5}	9.87×10^{-6}	0.651	1.49
	0.00373	2.57×10^{-5}	2.25×10^{-4}	3.46×10^{-5}	2.28	1.55
	0.0107	7.34×10^{-5}	6.42×10^{-4}	9.87×10^{-5}	6.51	1.99
	0.0426	2.94×10^{-4}	2.57×10^{-3}	3.95×10^{-4}	26.04	9.57
$B = 0.873T$	ΔT_r (K)	$ v_{r \max} $ (cm/s)	$ v_{z \max} $ (cm/s)	U (cm/s)	effective Pe_m	$D \times 10^5$ (cm^2/s)
$Ha = 100$	0.00171	2.85×10^{-6}	7.48×10^{-5}	9.87×10^{-7}	0.758	1.49
	0.00501	8.35×10^{-6}	2.19×10^{-4}	2.89×10^{-6}	2.22	1.55
	0.0171	2.85×10^{-5}	7.48×10^{-4}	9.87×10^{-6}	7.58	2.11
	0.0854	1.43×10^{-4}	3.74×10^{-3}	4.93×10^{-5}	37.9	16.0

Case II: uniform flux ~ periodic flux; $d = 0.01$, $e = 1$ and $n = 3$ in Eq. (1)

$B = 0.218T$ $Ha = 25$	ΔT_r (K)	$ v_{r \max} $ (cm/s)	$ v_{z \max} $ (cm/s)	U (cm/s)	effective Pe_m	$D \times 10^5$ (cm ² /s)
	0.00533	8.78×10^{-6}	6.41×10^{-5}	4.93×10^{-5}	0.652	1.49
	0.0249	4.11×10^{-5}	3.00×10^{-4}	2.31×10^{-4}	3.04	1.55
	0.0639	1.05×10^{-4}	7.70×10^{-4}	5.92×10^{-4}	7.82	1.84
$B = 0.873T$ $Ha = 100$	ΔT_r (K)	$ v_{r \max} $ (cm/s)	$ v_{z \max} $ (cm/s)	U (cm/s)	effective Pe_m	$D \times 10^5$ (cm ² /s)
	0.0427	8.46×10^{-6}	6.04×10^{-5}	2.47×10^{-5}	0.612	1.49
	0.171	3.38×10^{-5}	2.42×10^{-4}	9.87×10^{-5}	2.45	1.55
	0.684	1.35×10^{-4}	9.67×10^{-4}	3.95×10^{-4}	9.79	2.2

Case III: uniform flux ~ 100 * periodic flux; $d = e = 1$ and $n = 3$ in Eq. (1)

$B = 0.218T$ $Ha = 25$	ΔT_r (K)	$ v_{r \max} $ (cm/s)	$ v_{z \max} $ (cm/s)	U (cm/s)	effective Pe_m	$D \times 10^5$ (cm ² /s)
	0.00107	5.92×10^{-6}	7.56×10^{-5}	9.87×10^{-6}	0.766	1.49
	0.00373	2.07×10^{-5}	2.65×10^{-4}	3.45×10^{-5}	2.68	1.55
	0.0107	5.92×10^{-5}	7.56×10^{-4}	9.87×10^{-5}	7.66	1.99
$B = 0.873T$ $Ha = 100$	ΔT_r (K)	$ v_{r \max} $ (cm/s)	$ v_{z \max} $ (cm/s)	U (cm/s)	effective Pe_m	$D \times 10^5$ (cm ² /s)
	0.00171	2.83×10^{-6}	7.64×10^{-5}	9.87×10^{-7}	0.774	1.49
	0.00548	9.07×10^{-6}	2.45×10^{-4}	3.16×10^{-6}	2.48	1.55
	0.0171	2.83×10^{-5}	7.64×10^{-4}	9.87×10^{-6}	7.74	2.12

Case IV: 10 * uniform flux ~ periodic flux; $d = 0.001$, $e = 1$ and $n = 3$ in Eq. (1)

$B = 0.218T$ $Ha = 25$	ΔT_r (K)	$ v_{r \max} $ (cm/s)	$ v_{z \max} $ (cm/s)	U (cm/s)	effective Pe_m	$D \times 10^5$ (cm ² /s)
	0.00533	8.78×10^{-6}	6.17×10^{-5}	4.93×10^{-5}	0.624	1.49
	0.0262	4.31×10^{-5}	3.03×10^{-4}	2.42×10^{-4}	3.07	1.55
	0.0639	1.05×10^{-4}	7.40×10^{-4}	5.92×10^{-4}	7.50	1.84
$B = 0.873T$ $Ha = 100$	ΔT_r (K)	$ v_{r \max} $ (cm/s)	$ v_{z \max} $ (cm/s)	U (cm/s)	effective Pe_m	$D \times 10^5$ (cm ² /s)
	0.0427	8.61×10^{-6}	5.06×10^{-5}	2.47×10^{-5}	0.513	1.49
	0.184	3.71×10^{-5}	2.18×10^{-4}	1.06×10^{-4}	2.21	1.55
	0.513	1.03×10^{-4}	6.07×10^{-4}	2.96×10^{-4}	6.15	1.87

Case V: uniform flux \sim periodic flux; $d = 0.01$, $e = 1$ and $n = 2$ in Eq. (1)

$B = 0.218T$	ΔT_r (K)	$ v_{r \max} $ (cm/s)	$ v_{z \max} $ (cm/s)	U (cm/s)	effective Pe_m	$D \times 10^5$ (cm ² /s)
$Ha = 25$	0.0107	1.04×10^{-5}	8.39×10^{-5}	9.87×10^{-5}	0.850	1.49
	0.0426	4.14×10^{-5}	3.35×10^{-4}	3.95×10^{-4}	3.40	1.55
	0.107	1.04×10^{-4}	8.39×10^{-4}	9.87×10^{-4}	8.50	1.86
$B = 0.873T$	ΔT_r (K)	$ v_{r \max} $ (cm/s)	$ v_{z \max} $ (cm/s)	U (cm/s)	effective Pe_m	$D \times 10^5$ (cm ² /s)
$Ha = 100$	0.0854	1.00×10^{-5}	6.91×10^{-5}	4.93×10^{-5}	0.700	1.49
	0.222	2.60×10^{-5}	1.80×10^{-4}	1.28×10^{-4}	1.82	1.55
	0.854	1.00×10^{-4}	6.91×10^{-4}	4.93×10^{-4}	7.00	2.26

In all cases, the value of the simulated diffusivity increased with increasing effective Pe_m (i.e., with increasing temperature difference, and, thus, convective velocity magnitude). The dependence of the transport conditions on the nature of the thermal boundary conditions was such that for a uniform heat flux along the sidewall which produces a radial temperature difference in the liquid, the diffusivity vs. Pe_m were indistinguishable for $Ha = 25$ and 100. The diffusivities for $Ha = 100$ were higher than those for $Ha = 25$ in the presence of a periodic temperature profile produced by a periodic heat flux superimposed on a uniform heat flux (Cases II, III, IV, and V).

Case I which is uniform heat flux only (i.e., the radial temperature difference in the liquid is the only driving force) seems to be the most sensitive while Case V is the least sensitive among five different conditions considered in this model. From the results, one can conclude that a particular temperature profile at the sidewall (produced by a combination of uniform and non-uniform heat fluxes) is required to result in desired diffusivities (i.e., to operate within the allowable temperature non-uniformities) in self-diffusion experiments for this numerical model. For a fixed value of effective Pe_m , ΔT_r increases with increasing Ha (the magnetic field strength). Thus, stronger magnetic fields can tolerate a stronger driving force ΔT_r in self-diffusivity measurements for same convective conditions.

Acknowledgements

The support by National Aeronautics and Space Administration through Grants NCC8-99 and NAG8-1476 for this research is gratefully acknowledged. We are very thankful to Professor J. S. Walker at University of Illinois at Urbana-Champaign for his suggestions and help. Thanks also go to Lynne Carver for preparation of figures.

References

1. J. D. Verhoeven, *Trans. Met. Soc. AIME*. **242**: 1937 (1968).
2. J. I. D. Alexander, J. -F. Ramus, and F. Rosenberger, *Microgravity Sci. Tech.* **9**: 158 (1996).
3. J. I. D. Alexander and R. M. Banish, *Microgravity Sci. Tech.* **11**: 90 (1998).
4. L. N. Hjellming and J. S. Walker, *J. Fluid Mech.* **164**: 237 (1986).
5. N. Ma and J. S. Walker, *Phys. Fluids*. **9**: 1182 (1997).
6. N. Ma, K. O. Homan, and J. S. Walker, *Phys. Fluids*. **9**: 2789 (1997).
7. W. V. Youdelis, D. R. Colton, and J. Cahoon, *Can. J. Phys.* **42**: 2217 (1964).

8. T. Alboussiere, J. P. Garandet, P. Lehmann, and R. Moreau, *Fluid Mechanics and its Applications: Transfer Phenomena in Magnetohydrodynamic and Electroconducting Flows*, Vol. **51** (Kluwer, New York, 1999), pp. 359-372.
9. Y. Y. Khine and J. S. Walker, *J. Crystal Growth* **147**: 313 (1995).
10. C. Canuto, M. Y. Hassaini, A. Quarteroni, and T. A. Zang, *Spectral Methods in Fluid Dynamics*, 3rd Ed. (Springer-Verlag, New York, 1988).
11. P. Codastefano, A. Di Russo, and V. Zanza, *Rev. Sci. Instrum.* **48**: 1650 (1977).
12. H. S. Harned and R. L. Nuttall, *J. Am. Chem. Soc.* **69**: 736 (1947).
13. T. Ida and R. I. L. Guthrie, *The Physical Properties of Liquid Metals* (Clarendon, Oxford, 1988).